The IgCAM BT-IgSF (IgSF11) is essential for connexin43-mediated astrocyte-astrocyte and ependymal cell-cell coupling

Laura Pelz[1,2)], Laura Dossou[1,3)] , Nine Kompier[1)], René Jüttner[1)], Gabrielle Siemonsmeier[1,4)], Niklas Meyer[1,5)], Elijah D. Lowenstein[1)], Ines Lahmann[1)], Helmut Kettenmann[1)], Carmen Birchmeier[1)], and Fritz G. Rathjen[1,7)]

1) Max-Delbrück-Center for Molecular Medicine, Robert-Rössle-Str. 10, DE-13092 Berlin, Germany
2) Present address: National Center for Tumor Diseases (NCT) Heidelberg and the German Cancer Research Center (DKFZ), Im Neuenheimer Feld 460, 69120 Heidelberg, Germany.
3) Present address: Pfizer Pharma GmbH, Linkstraße 10, 10785 Berlin, Germany
4) Present address: McGill University, Integrated Program in Neuroscience, Irving Ludmer Building, 1033 Pine Avenue West, Montréal, Québec H3A 1A1, Canada
5) Present address: Department of Microbiology, Oslo University Hospital, Sognsvannsveien 20, 02770 Oslo, Norway
7) Correspondence: Fritz G. Rathjen (rathjen@mdc-berlin.de)

Running title: BT-IgSF and connexin43-mediated astrocyte-astrocyte coupling

Key words: IgCAM, BT-IgSF, gap junctions, connexin43, cell-cell coupling

Summary statement

In the brain astrocytes are organized in vast networks communicating through gap-junctions. Here, we demonstrate that the cell adhesion molecule BT-IgSF controls connexin43-mediated coupling in astrocytes and ependymal cells.

Abstract

The type I transmembrane protein BT-IgSF is predominantly localized in the testes and brain. It belongs to the CAR subgroup of Ig cell adhesion proteins, which have been hypothesized to regulate connexin expression or localization. Here, we studied the putative link between mouse BT-IgSF and connexins in astrocytes, ependymal cells and neurons of the mouse. Global knockout of BT-IgSF caused an increase in the clustering of connexin43 (Gja1), but not of connexin30 (Gjb6), on astrocytes and ependymal cells. Additionally, we also found reduced expression levels of connexin43 protein in the cortex and hippocampus of knockout animals. Analysis of biocytin spread in hippocampal or cortical slices from mature mice of either sex revealed a decrease in astrocytic cell-cell coupling in the absence of BT-IgSF. The localization and expression of connexin36 (Gjd2) on neurons was not affected by the absence of BT-IgSF. Overall, our data indicate that the IgCAM BT-IgSF is essential for correct gap junction-mediated astrocyte-to-astrocyte and ependymal cell-to-ependymal cell communication. These data are discussed in the context of results obtained with knockouts of other members of the CAR protein subgroup.

Introduction

BT-IgSF (brain- and testis-specific Ig superfamily protein, also known as IgSF11) is a cell adhesion protein belonging to a small group of IgCAMs consisting of CAR (coxsackievirus and adenovirus receptor), ESAM (endothelial cell-selective adhesion molecule) and CLMP (CAR-like membrane protein). The group shares a similar overall domain organization with an N-terminal V-type and a C2-type Ig domain and a highly related amino acid sequence (Rathjen, 2020). Initially BT-IgSF was described as a novel IgSF member that was preferentially expressed in the brain and testis (Suzu et al., 2002). Independently of this report BT-IgSF was also found to be up-regulated in intestinal-type gastric cancers and termed IgSF11 (Katoh and Katoh, 2003) (moreover it was also termed V-set and Immunoglobulin domain containing 3, abbreviated VSIG-3) (Harada et al., 2005; Wang et al., 2018). The cytoplasmic segment of BT-IgSF contains a PDZ-binding motif at its C-terminus that interacts with the scaffolding protein PSD95 (Jang et al., 2015). Adhesion assays with heterologous cells showed that BT-IgSF promotes the homotypic cell binding (Eom et al., 2012; Harada et al., 2005).

So far, the function of BT-IgSF (IgSF11) has been studied in neurons, Sertoli and germ cells of the testes, during osteoclast differentiation and in the organization of pigment cells in fish (Ahi and Sefc, 2017; Chen et al., 2021; Eom et al., 2012; Hayano et al., 2021; Jang et al., 2015; Kim et al., 2020; Pelz et al., 2017; Singh and Nusslein-Volhard, 2015). Knockdown studies using cultured mouse hippocampal neurons indicated that BT-IgSF is implicated in synaptic transmission through a tripartite interaction with PSD95 and AMPA receptors (Jang et al., 2015). Consequently, global BT-IgSF-deficient mice displayed a moderately decreased excitatory synaptic strength in the dentate gyrus and long-term potentiation in hippocampal CA1 (Jang et al., 2015). In another study in neurons BT-IgSF was found to regulate the innervation of axons of chandelier cells on initial axon segments of pyramidal neurons (Hayano et al., 2021).

In the murine testis BT-IgSF is expressed in Sertoli cells at the blood-testes barrier, a structure that opens and closes to allow the passage of germ cells. In a global knockout the absence of BT-IgSF causes a malfunction of the blood-testes-barrier leading to male infertility due to the mislocalization of connexin43. Connexin43 was found throughout the seminiferous epithelium instead of being restricted to the blood-testes barrier as it is in wild type animals. Therefore BT-IgSF might regulate the localization or activity of connexin43 in Sertoli cells (Pelz et al., 2017). In line with this finding is that connexin43 plays an essential role in tight junction reassembly at the blood-testes barrier during its restructuring processes (Li et al., 2010). A critical role of BT-IgSF in regulating the organization of pigment cells into stripes along the dorso-ventral or anterior-posterior body axes was observed in zebrafish and *Neolamprologus meeli* (Ahi and Sefc, 2017; Eom et al., 2012; Singh and Nusslein-Volhard, 2015). Similar irregular patterns of chromatophores have been described in zebrafish with mutations in the genes of connexin 41.8 and connexin39.4 suggesting a functional link between BT-IgSF and connexins (Haffter et al., 1996; Irion et al., 2014; Watanabe and Kondo, 2012; Watanabe et al., 2006). Together, these data suggest an essential function of BT-IgSF in regulating the localization or activity of connexins as it has been discussed for other members of the CAR subgroup (Rathjen, 2020).

To get further evidence for a functional interaction between interaction between BT-IgSF and connexin43 we investigated its role on glial cells. Here, we show that BT-IgSF is strongly localized on the surface of astrocytes and ependymal cells in addition to its previously described neuronal expression (Higashine et al., 2018; Jang et al., 2015; Suzu et al., 2002). In the absence of BT-IgSF in a global knockout we demonstrate the aberrant clustered localization of connexin43 on astrocytes and ependymal cells and a severe reduction in connexin43 at the protein level. Consequently, dye loading experiments revealed reduced diffusion within the astrocytic network in the hippocampus as well as in the cortex of mutant mice. We discuss our findings in the context of the function of the related proteins CLMP and CAR which also affect the expression and localization of connexin43 and 45 in the smooth muscle cells of the intestine and in cardiomyocytes, respectively (Langhorst et al., 2018; Lim et al., 2008; Lisewski et al., 2008; Rathjen, 2020).

Results

Absence of BT-IgSF disrupts the expression and the localization of connexin43 in the hippocampus and on ultured astrocytes

Our previous studies showed connexin43 mislocalization in Sertoli cells of the testes in BT-IgSF-deficient mice, indicating a functional interaction of the IgCAM BT-IgSF and connexin43 (Pelz et al., 2017). Extending these observations, here we focused on the role of BT-IgSF and connexin43 localization in the brain of BT-IgSF-deleted mice. In the nervous system connexin43 is known to be expressed by astrocytes and ependymal cells, but not neurons. Connexin30 and connexin26 have also been detected in adult astrocytes, albeit at lower levels (Dermietzel et al., 1989; Nagy et al., 2004). Astrocytes are organized in vast networks that facilitate extensive intercellular communication through gap-junction channels formed by connexins (Fischer and Kettenmann, 1985; Giaume et al., 2010; Kettenmann et al., 1983), and therefore may be an appropriate cell type to investigate a functional link between BT-IgSF and connexin43. Accordingly, in monolayer cultures prepared from newborn hippocampal tissue BT-IgSF was primarily localized on the surface of GFAP-positive astrocytes (Figure 1A and B and Supplementary Figure S1 on the specificity of the anti-BT-IgSF antibody) and was not or only weakly detected on MAP2-positive dendrites (Figure 1C). However, RNAscope in situ hybridization experiments indicated that neurons express detectable amounts of BT-IgSF mRNA (see below). Similarly, BT-IgSF mRNA was found in GFAP–positive cells in sections of the molecular layer of the hippocampus (Figure 1E and F) which is further supported by immunohistochemistry using polyclonal antibodies to the extracellular region of BT-IgSF (Figure 1D). BT-IgSF protein expression increases as the brain matures postnatally and for effective solubilization from crude membrane fractions requires ionic detergents such as SDS (Figure 1G and H).

On the basis of the localization of BT-IgSF in astrocytes we tested whether the absence of BT-IgSF also affects the localization or level of connexin43 expression on astrocytes as it was found in the testes (Pelz et al., 2017). Hippocampal sections as well as astrocyte monolayer cultures were labeled with rabbit anti-connexin43 antibodies. Microscopic images of hippocampal sections revealed an altered localization of connexin43 in the BT-IgSF knockout tissue (Figure 2A and B). High power magnifications demonstrated a severe decrease in the number of connexin43 spots (31% of the wild type) and a considerable increase in the connexin43 spot size (from 0.19 to 0.5 μm^2 on average) in the molecular layer of knockout hippocampal tissue (Figure 2C, E and F). Similar observations on the clustering and number of connexin43 spots were made on cultured astrocytes, suggesting that BT-IgSF might control connexin43 localization even in the absence of neurons (Figure 2D, H and I). Analysis of the distribution of the number of counts versus cluster size further highlights the difference between wild type and knockouts (Figure 2G and J). Taken together our data indicate that BT-IgSF is essential for the correct subcellular localization and clustering of connexin43 in astrocytes.

To analyze connexin43 in Western blots, hippocampus or cortex crude membrane fractions from wild types and mutants were prepared. Membranes were first treated by Triton X100 followed by SDS of the pellet to separate soluble (primarily non-junctional) from insoluble (mainly junctional) connexin43 (Figure 3A and B). Significant decreases in

connexin43 levels in both TX100- and SDS-containing fractions were found in the mutant. No changes were detected for GFAP at the protein level (Figure 3D) or for the number of GFAP-positive astrocytes (Figure 4I) in the hippocampus of BT-IgSF mutants. This indicated that the reduction in connexin43 level was not caused by a decrease in the number of GFAP-positive cells. In contrast to connexin43, connexin30, which is also implicated in the extensive network organization of astrocytes and which can also form gap junction channels together with connexin43 (Nagy et al., 2004; Willecke et al., 2002), is not reduced nor is its clustering changed in the hippocampus in the absence of BT-IgSF (Figure 3A and C).

Taken together these data indicate that BT-IgSF is also essential for the expression of connexin43 protein in astrocytes.

Reduced astrocyte-astrocyte coupling in the hippocampus and cortex in the absence of BT-IgSF

A typical feature of astrocytes is their organization in vast networks that communicate with one another via gap-junction channels formed by connexins (Giaume et al., 2010). In order to investigate the effect of the BT-IgSF knockout on astrocytic network size in the hippocampus and cortex we performed dye-coupling experiments (Scheme shown in Figure 4A). Astrocytes were identified in acutely isolated mouse brain slices by sulforhodamine 101 labelling as a specific marker of astroglia (Nimmerjahn et al., 2004). Individual astrocytes in the hippocampus molecular layer region or cortical layers II – IV from horizontal slices were dye-loaded with biocytin for 20 minutes via patch pipette. Diffusion of the dye throughout the astrocytic network allows for the visualization and quantification of the extent of gap-junction mediated cell-cell coupling (Figure 4B).

In the hippocampus as well as in the cortex, the number of coupled astrocytes per injected cell was significantly decreased in mutant animals. 16 dye-filled slices from 4 control mice and 11 slices from 3 BT-IgSF knockout mice were used for immunohistochemical analysis of hippocampal coupled astrocytic networks. On average 101 (SEM ± 8.851) biocytin-positive hippocampal astrocytes were detected to be coupled in the wild type, whereas in the knockout only 78 (SEM ± 7.837) biocytin-positive astrocytes are found to form a network (Figure 4C to E). In the cortex the differences between wild type and knockout were even more pronounced: on average 118 (SEM ± 20.95) astrocytes in control and only 48 (SEM ± 7.86) in the BT-IgSF knockout form a network (11 dye-filled slices from 4 control and 10 slices from 4 knockouts were used here) (Figure 4F to H). Supplementary Figure S2 illustrates the passive membrane properties of hippocampal astrocytes in both groups over the course of the dialysis period. We observed no significant differences in the current to voltage relationship, membrane resistance or membrane capacitance ($p>0.05$) between genotypes or between the start and the end of the dialysis period. This indicated that a change in the astrocytic network extent was not due to these factors. Similar results were obtained for passive membrane properties in cortical astrocytes (not shown). Further, neither the density of GFAP-positive astrocytes nor their complexity (arborization) was reduced in the absence of BT-IgSF, suggesting that altered morphological parameters of astrocytes are unlikely to cause the reduced cell-cell coupling in the absence of BT-IgSF (Figure 4I to K).

In summary, we detected a significantly reduced astrocyte-astrocyte coupling in the hippocampus and the cortex in the absence of BT-IgSF. This could be due to the reduced

connexin43 expression at the protein level, a decrease in the number of puncta or its altered subcellular localization.

Absence of BT-IgSF disrupts the localization of connexin43 on ependymal cells

Ependymal cells are specialized cells that line the ventricles and form an interface between the cerebrospinal fluid (CSF) and brain parenchyma. Ependymal cells contact each other via connexin43 containing gap junctions and are implicated in the production and circulation of cerebrospinal fluid as well as barrier formation (Saunders et al., 2018). To ask whether the absence of BT-IgSF also affects the localization of connexin43 on ependymal cells we characterized the expression of BT-IgSF in the brain by immunohistochemistry. In cryostat sections we detected a strong localization of BT-IgSF on cells lining all brain ventricles at embryonic as well as postnatal stages, but only very weak staining in the neural tissue directly adjacent to the ependymal cell layer (Figure 5A, see also supplementary Figure S3 for antibody specificity). At higher magnifications BT-IgSF was found at the lateral and basal surfaces of ependymal cells, but was absent from the apical side that faces the ventricle (Figure 5B). The choroid plexus which expresses the related IgCAM CAR was found to be negative for BT-IgSF (Figure 5C). Matching the deficits that we found in astrocytes, we also found increased clustering of connexin43 in ependymal cells in BT-IgSF mutants in comparison to wildtypes, suggesting that their cell-cell coupling could also be affected (Figure 5 D to G).

The localization of connexin36 in neurons is not affected by the absence of BT-IgSF

Next, we asked whether the absence of BT-IgSF also affects the localization of the neuronal gap junction protein connexin36. While connexin43 is restricted to astrocytes, connexin36 is the main connexin in neurons, and is primarily expressed during embryonic and early postnatal developmental stages (Condorelli et al., 1998; Degen et al., 2004; Gulisano et al., 2000; Rubio and Nagy, 2015; Söhl et al., 1998). While we experienced that commercially available antibodies to connexin36 were of limited use in our hands, we generated a polyclonal antibody to the cytoplasmic stretch (residues 99 to 197) of mouse connexin36 (Figure 6 A - D). Although this antibody also showed some unspecific binding it clearly labeled connexin36 at a molecular mass of 34 kD in wildtype but not in connexin36-deficient neural tissues in Western blots (Figure 6D). The strongest expression of connexin36 was detected in the midbrain and hindbrain at postnatal day 10, while much weaker expression levels were found in the cerebellum, basal ganglia, hippocampus and cortex. The specificity of this antibody to connexin36 could be demonstrated in cryostat sections of wildtype or connexin36-deficient tissue Figure 6E). *BT-IgSF* encoding mRNAs were found to be co-expressed by *vGlut1* and *GAD65*-positive cells in the midbrain, indicating expression in both excitatory and inhibitory neurons (Figure 6F). Similar expression patterns were seen in the hippocampus (Supplementary Figure S4). Since the strongest expression of connexin36 was detected in the midbrain, the pattern of expression was studied in this region. Interestingly, no differences in the localization or expression of connexin36 were detected in the absence of BT-IgSF in the midbrain (Figure 6G and H). We conclude that BT-IgSF modulates the

expression of connexin43 specifically in astrocytes and ependymal cells and does not interfere with the localization or clustering of connexin36 in neurons.

Discussion

In this study we demonstrated that the Ig cell adhesion molecule BT-IgSF is highly expressed on astrocytes and ependymal cells of the mouse brain. It is essential for the correct expression and subcellular localization of connexin43, but not connexin30, in astrocytes and ependymal cells. Both connexins form gap junctions in astrocytes consisting of densely packed transmembrane channels that allow for direct cell-to-cell communication. Disruptions of gap junction coupling are found in several diseases (Huang et al., 2021; Mayorquin et al., 2018). In the absence of BT-IgSF the level of connexin43 protein is severely reduced and surprisingly larger plaque sizes of connexin43 are formed on their cell surfaces in comparison to wild type littermates. In contrast, a change in the pattern of localization or level of expression of connexin36 in neurons was not detected in the absence of BT-IgSF. Astrocytes generate a complex syncytial network allowing them to interact with many neighboring cells to control a number of physiological processes (Mazaud et al., 2021). Our analysis of gap junction coupling analyzed by dye diffusion revealed a reduced astrocytic network in the hippocampus and cortex in BT-IgSF knockouts. However, this impaired coupling was not due to morphological changes of astrocytes in the absence of BT-IgSF.

BT-IgSF is a member of a small and evolutionarily conserved subfamily of IgCAMs of which CAR was the founding member. This set of proteins mediates homotypic cell adhesion, share a common overall extracellular domain structure and are highly related at the level of amino acid sequence. A number of findings by mouse knockout studies suggested that these proteins might undertake similar functions in that they help to organize or regulate gap junctions in a variety of cell types (Falk, 2020; Rathjen, 2020). For example, in the absence of CAR connexin43 and 45 are reduced in the heart, leading to impaired electrical conduction at the atrioventricular node as indicated by a prolonged PR interval (Lim et al., 2008; Lisewski et al., 2008). Another example is CLMP: the absence of this adhesion protein impaired smooth muscle cells of the intestine and ureter. Uncoordinated calcium signaling provoked a disturbed contraction of the intestine and ureter causing severe bilateral hydronephrosis and a high rate of mortality due to the insufficient transport of chyme and urine. Notably, the level of connexin43 and 45 protein but not their mRNA was severely reduced in the smooth muscle layers in CLMP-deficient mice (Langhorst et al., 2018), which is very similar to the CAR conditional knockout phenotype in the heart mentioned above. Our studies on BT-IgSF described here provide an additional example of the way this subgroup of proteins plays a part in gap junction mediated cell-cell communication. The absence of BT-IgSF also affects the expression and localization pattern of connexin43 in astrocytes and ependymal cells. This is consistent with our previously published data on the mislocalization of connexin43 in Sertoli cells of the testes, which leads to infertility and the functional impairment of the blood-testes-barrier (Pelz et al., 2017).

How might BT-IgSF exert its function on connexin43 in astrocytes?

Connexin43, much like other connexins, has a dynamic "life cycle" with a half-life time of about one to five hours. Furthermore, connexin biosynthesis is complex and a plethora of proteins are known to interact with connexins during all stages of the gap junction life cycle (Solan and Lampe, 2016). Reduced astrocyte-astrocyte coupling was also recently described in knockdown experiments of the Ig cell adhesion molecule HepaCAM (also termed GlialCAM) which is only distantly related to CAR subgroup members at the structural level. The authors found a reduced morphological complexity, including arborization of astrocytic protrusions, and a reduction in the territory covered by astrocytes. In addition, an increased clustering of connexin43 was found in HepaCAM knockouts. Altogether this caused a decrease in dye coupling (Baldwin et al., 2021). Except for the increased clustering of connexin43 here we did not detect similar morphological changes in astrocytes of BT-IgSF knockouts, nor did we find a reduction in the cell density in the molecular layer of the hippocampus. Therefore, in astrocytes HepaCAM and BT-IgSF seemingly play different roles, although in both cases their mutation resulted in impaired coupling. Furthermore, in biochemical experiments a direct association of HepaCAM with connexin43 at the cell surface was established (Baldwin et al., 2021; Wu et al., 2016). By contrast, based on our preliminary co-localization studies in cultured astrocytes, we only occasionally detected the close proximity of BT-IgSF with connexin43 at the cell surface of astrocytes.

Co-localization of BT-IgSF with the scaffolding protein ZO-1 (Zona Occludens-1) at the cell surface of Sertoli cells was detected in Sertoli cells in confocal images (Pelz et al., 2017). BT-IgSF harbors a PDZ binding motif at its C-terminal domain and scaffolding proteins such as ZO-1 bind via a PDZ domain to most connexins (Hervé et al., 2014). Therefore, one might speculate that ZO-1 binds to BT-IgSF via its PDZ domain1 and to connexin43 via its PDZ domain 2 to regulate connexin43 localization at the plasma membrane (Duffy et al., 2002). Furthermore, ZO-1 has been shown to control gap junction assembly and localization and influences plaque size in cell cultures (Hunter et al., 2005; Laing et al., 2005; Rhett et al., 2008). In addition, a frameshift mutation in the connexin43 gene in human patients suffering from oculo-dento-digital dysplasia disrupts the connexin43-ZO-1 interaction (Bock et al., 2013; van Steensel et al., 2005). Despite these findings in other cell types, in our unpublished studies co-localization of ZO-1 with connexin43 or co-localization of BT-IgSF with connexin43 was only occasionally detected at the plasma membrane of astrocytes. Therefore, a transient association of these components is conceivable. However, additional studies with mice expressing mutant versions of genes affecting the interactions between BT-IgSF and ZO-1 and between ZO-1 and connexin43 might clarify whether these complexes are indeed formed and if they play a role for connexin43 assembly in astrocytes. Currently the question how BT-IgSF controls connexin43 localization remains unanswered. Further studies are needed to thoroughly understand the signal transduction pathways downstream of BT-IgSF that modulate the de novo incorporation of connexin43 into the plasma membrane.

BT-IgSF might have different functions in neurons and glial cells

Previously published knockdown studies using cultured hippocampal neurons implicated BT-IgSF (IgSF11) in synaptic transmission through interactions with PSD95 and AMPA receptors in the CA1 region of the hippocampus (Jang et al., 2015). In these *in vitro*

experiments knockdown of BT-IgSF (IgSF11) caused an increased mobility and endocytosis of AMPA receptors suggesting that BT-IgSF is important for the stabilization of AMPA receptors in the neuronal plasma membrane. Consequently, BT-IgSF-deficient mice revealed a moderately decreased excitatory synaptic strength in the dentate gyrus and enhanced long-term potentiation in CA1 (Jang et al., 2015). To verify if our findings specifically apply to astrocytic connexin43 we studied the localization and expression of connexin36 which is the main connexin expressed in neurons (Condorelli et al., 1998; Degen et al., 2004; Gulisano et al., 2000; Rubio and Nagy, 2015; Söhl et al., 1998). Highest expression of connexin36 was found in the midbrain and hindbrain at early postnatal stages. Therefore, the localization and level of expression of connexin36 was studied in these structures. Interestingly, no significant differences in the localization pattern or expression of connexin36 at the protein level were detected in the absence of BT-IgSF in the midbrain. We conclude that BT-IgSF might have a different function in astrocytes and neurons, specifically modulating the expression of connexin43 in astrocytes and ependymal cells, but not affecting the pattern of connexin36 in neurons.

What might be the consequences of astrocyte network disturbance for neuronal function?

Astrocytes form an elaborate network to control a number of physiological processes in the brain. Disrupted communication of astrocytes in the absence of BT-IgSF might therefore interfere with the coordination of astrocytic calcium waves or might affect synaptic activity. The close contact of astrocytic branches with synapses allows astrocytes to sense neuronal activity via their ion channels and neurotransmitter receptors (Ventura and Harris, 1999). Disruption of astrocytic networks for example by inactivation of connexin43 and 30 reduced synaptic transmission (Charvériat et al., 2017; Giaume et al., 2010; Hardy et al., 2021; Pannasch et al., 2011; Perea et al., 2009; Pereda, 2014). Accordingly, connexin30 and astrocyte-targeted connexin43 knockout mice as well as connexin43 and 30 double knockout mice display impaired performance in sensorimotor and spatial memory tasks (Lutz et al., 2009; Theis et al., 2003). Astrocyte coupling is also altered in epilepsy (Steinhäuser and Boison, 2012). Decreased coupling among astrocytes promotes neuronal hyperexcitability and attenuates seizure-induced histopathological outcomes (Deshpande et al., 2020). Astrocytic dysfunction is implicated in a number of neurodevelopmental disorders (Molofsk et al., 2012; Tan et al., 2021).

In the brain and spinal cord, ependymal cells line the ventricles and bear multiple cilia which beat in a concerted manner at their apical surface to drive cerebrospinal fluid circulation (Spassky and Meunier, 2017). This unidirectional movement might be coordinated by gap junction mediated cell-cell communication. Consistent with this hypothesis, *zebrafish* embryos injected with connexin43 morpholinos and connexin43-deficient mouse embryos exhibit a decreased number of cilia as well as diminished beating (Zhang et al., 2020).

In conclusion, in the present study we have identified BT-IgSF as a crucial molecular helper to establish correct localization of connexin43 on astrocytes and ependymal cells; in astrocytes, this is essential for effective cell-cell coupling. Whether BT-IgSF's selective absence in astrocytes or ependymal cells is also important for neurotransmission or the coordinated movement of cilia, respectively, should be investigated in future work.

Material and Methods

Mice

The global knockout of BT-IgSF (B6-Igsf11$^{tm1e(KOMP)Wtsi}$/FGR) and its genotyping has been described elsewhere (Pelz et al., 2017). Breeding was either from tg/wt to tg/wt or tg/tg (female) to wt/tg (male). Heterozygous BT-IgSF mice did not differ from wt/wt mice (Pelz et al., 2017). Cx36-deficient mice (B6.129P2-Gjd2tm1Kwi/Cnrm; EM:00326) were obtained from the European Mouse Mutant Archive (EMMA) and genotyped as described (Güldenagel et al., 2001). Animals were housed on a 12/12 h light/dark cycle with free access to food and water. The animal procedures were performed according to the guidelines from directive 2010/63/EU of the European Parliament on the protection of animals used for scientific purposes. All experiments were approved by the local authorities of Berlin (LaGeSO) (numbers T0313/97, X 9007/16, O 0038/08 and H0027/20). Wild type littermates served as controls.

Cell culture, antibodies and immunocytochemistry

Hippocampal cells were prepared from postnatal day 2 or 3 mice and cultured on poly-D-lysine coated coverslips in 24-well plates at a density of 7.5 x 10^4 cells/ml in Neurobasal (Invitrogen) supplemented with B27 (Invitrogen) and 10% FCS (Gibco) for 10 days. Every third day half of the culture medium was removed and replaced by Neurobasal/B27 without FCS. Glial cells from postnatal day 2/3 cortices or hippocampi were prepared according to standard procedures and were maintained in DMEM supplemented with 10% FCS and penicillin/streptomycin (McCarthy and De Vellis, 1980). For immunocytochemistry cells were fixed in 4% paraformaldehyde/PBS for 10 minutes, washed with PBS/1% BSA. For stainings of cryosections (thickness 12-16 µm) by indirect immunofluorescence, adult mice were transcardially perfused with 50 ml PBS followed by 50 ml 4% paraformaldehyde. Brains were post fixed for 5 hours and then transferred into 15% followed by 30% (w/v) sucrose in PBS to obtain cryoprotection. Primary and fluorophore-conjugated secondary antibodies were applied in blocking solution (3% goat or donkey serum, 1% BSA, 0.1% Triton X-100 in PBS). Mouse monoclonal antibodies were incubated on sections using the MOM immunodetection kit from Vector Laboratories (BMK-2202). Sections or monolayer cultures were counterstained with the nuclear stain DAPI at 1 µg/ml. For antibodies see table 1.

Microscopic images were obtained at room temperature by confocal imaging using a Carl Zeiss LSM 700 Laser Scanning Microscope equipped with ZEN 2011 software and the following lenses: a Plan-Neofluar 20x/0.30 NA objective, a Plan-Achromat 40x/1.3 Oil, a Plan-Achromat 63x/1.40 NA oil objective or a Plan Apochrome 100x/1.40 oil objective (all from Carl Zeiss MicroImaging, GmbH). Figures were assembled using Illustrator CS5 (Adobe).

To quantify connexin43 clusters confocal images were taken with a 63x objective from cryosections and a 100x objective for cultured astrocytes. Quantification of connexin43 clusters was done by Fiji software setting threshold to RenyiEntropy routine; clusters were accepted between 0.05 and 1.00 µm^2 (2-40 pixels).

Generation of a connexin 36 fusion protein and polyclonal antibodies to connexin36.

Since several commercial anti-connexin36 antibodies were of limited use we generated polyclonal anti-mouse connexin36 antibodies in rabbits using a fusion protein that comprised the second cytoplasmic segment of mouse connexin36 (amino acid residues 99 – 197) attached to a histidine stretch. The cDNA of this segment was synthesized by Invitrogen and cloned into plasmid pMA-RQ and further subcloned into the bacterial expression vector pET-14b (Novagen/EMD Millipore). The protein was expressed in Bl21 bacteria with the addition of IPTG to a final concentration of 1 mM. Bacteria were harvested by centrifugation and frozen at 80^{o}C. Bacterial pellets were resuspended in ice-cold lysis buffer containing 2 M Urea, 50 mM Tris, 150 mM NaCl, pH 7.4, supplemented with protease blockers (aprotinin, PMSF, leupeptin, pepstatin). Unsolubilized material was removed by centrifugation and the supernatant was precipitated by ammonium sulfate (50% saturation). The pellet was dialyzed against 10 mM Tris, pH 11 and run over an anion exchange column (DE52 Whatman). The unbound fraction was applied to an NTA column (Qiagen), washed with 20 mM imidazole and bound protein was eluted by 200mM imidazole. Purity was analyzed by 15% SDS PAGE. Rabbits were injected with 100 µg protein in Freund's adjuvant at fortnightly intervals. The IgG fraction was obtained by protein A affinity chromatography (GE Health Care) and further purified by affinity chromatography on an affinity column containing the above mentioned connexin36 segment protein coupled to CNBr-activated Sepharose (14 mg to 2.5 g Sepharose 4B; GE Healthcare). The specificity of the affinity purified antibodies was tested on tissue extracts and cryostat sections (12 µm thick, mildly fixed with 1% paraformaldehyde/PBS for 1 minute on ice) from wild type or connexin36-deficient mice.

Biochemical methods

To obtain a crude membrane fraction from tissues of BT-IgSF knockout or wild type mice of different ages (as indicated in the Figure legends), hippocampi or cortices were homogenized in 0.34 M sucrose supplemented with protease blockers [aprotinin (20 U/µl), leupeptin (5 mM), pepstatin (5mM), PMSF (1mM)]. Nuclei were pelleted at 200xg for 10 minutes and the resulting supernatant was centrifuged at 100 000xg for 10 minutes to obtain a crude membrane pellet and cytoplasmic fraction in the supernatant. Membranes were stripped with 0.1 M diethylamine (pH11.5), supplemented with protease blockers to remove peripheral membrane proteins. The membrane fraction was first solubilized in 1% Triton X100 and unsolubilized material was removed by centrifugation. The pellet was then solved in 1% SDS in PBS supplemented with protease blockers and unsolubilized material was again removed by centrifugation. Protein concentrations were determined using the Bradford assay (Bio-Rad #500-0006) and spectrophotometric measurements. Equal amounts of proteins were loaded on SDS-PAGE for Western blotting which was controlled by Ponceau staining and h ouse keeping proteins such as GAPDH, heavy chain of clathrin, or α-tubulin. Depending on the tissue or antibody, 10, 15 or 20 µg of protein was loaded per lane. For the calculation of the molecular mass of connexin36 in neural tissues the following molecular mass standards were used (in kDa): Conalbumin, 76; BSA, 66¸actin, 43; GAPDH, 36 and carbonic anhydrase, 31.

RNAscope on hippocampus sections

In situ fluorescent hybridization was performed using the RNAscope Multiplex Fluorescent Assay from ACDbio according to the manufacturer's instructions (Wang et al., 2012). Briefly, PFA-fixed hippocampus or midbrain sections of 20 µm thickness were

obtained from P20 or P10 wild type mice, respectively, and stored at -80°C until use. Sections were thawed at 37°C for 10 mins and post-fixed in 4% PFA in PBS for 15 minutes before washing in PBS and continuing with the manufacturer's instructions. Protease treatment was performed using Protease IV. RNAscope probes against BT-IgSF (C1 - 451131), GFAP (C2 - 313211), vGlut1 (C2 - 416631) and GAD65 (C2 - 415071) were used.

Dye coupling in acute brain slices

To characterize the tracer spread within coupled astrocytic networks acute brain slices containing the hippocampus or the cortex were prepared from 8-10 week old knockout or littermate controls of either sex as described previously (Maglione et al., 2010). In brief, mice were sacrificed by cervical dislocation, decapitated and their brains carefully removed and mounted in a chamber with ice-cold bicarbonate-buffered artificial cerebrospinal fluid (ACSF), composed of (in mM): NaCl 134; KCl 2.5; $MgCl_2$ 1.3; $CaCl_2$ 2; K_2HPO_4 1.25; $NaHCO_3$ 26; D-glucose 10; pH 7.4. The buffer solution was continuously gassed with carbogen (95% O_2, 5% CO_2). Coronal slices of 250 µm were prepared at 4°C using a vibratome (HM 650 V, Microm International GmbH, Walldorf, Germany), and stored in ACSF at room temperature (21–25°C) for up to 5 hours.

Before dye filling, slices were incubated for 20 minutes in 1µM sulforhodamine 101 (SR-101) at 35°C to label astrocytes. Astrocytes were identified by their SR-101 fluorescence at excitation and emission wavelengths of 555 and 585 ± 10 nm, respectively, using a 60x water-immersion objective (Olympus, Hamburg, Germany). For recording and for dye loading, a patch pipette (pulled from borosilicate glass, 1.5 mm outside diameter, 0.315 mm wall thickness) was filled with a solution containing 30 mM KCl, 1 mM $MgCl_2$, 0.5 mM $CaCl_2$, 100 mM potassium-gluconate, 10 mM Hepes, 5 mM EGTA, 0.5% biocytin (Sigma-Aldrich) and 3 mM Na_2ATP, pH 7.3. Lucifer Yellow (10 µg/ml; Sigma-Aldrich) was added to the pipette solution and intracellular access of the solution was confirmed by excitation at 495 nm and visualization at an emission wavelength of 510 ± 10 nm. The pipette resistance ranged from 5 – 8 MΩ. Cells were passively dialyzed via the patch pipette for 20 min. In order to confirm cell identity and vitality, membrane currents were recorded with a series of de- and hyperpolarizing voltage steps (10 mV each, filtered at 2.9 kHz) from a holding potential of -70 mV ranging from -160 to +50 mV for 50 ms), using an EPC 10 patch-clamp amplifier and TIDA 5.25 software (HEKA Elektronik, Lambrecht, Germany), as described previously (Richter et al., 2014). Capacitive transients from the pipette were compensated online via the patch clamp amplifier (Cfast) whereas membrane capacity and series resistance (Cslow) were not compensated. The calculated liquid junction potential of the used intra cellular solutions was – 8.858 mV using Patchers Power Tools (Mendez & Würriehausen, Göttingen, Germany) and Igor Pro 7 software (Wavemetrics, Portland, OR, USA). The calculated reversal potentials of astrocytes were corrected for the liquid junction potential. Only cells whose series resistance was not higher than 125 % at the end of the dialysis phase compared to the beginning of the recording were taken into account for the following immunohistochemical experiments and the calculation of the membrane properties. After dye loading and patch-clamp recording, the pipette was carefully removed from the cell in order to disrupt the patch.

Slices were subsequently fixed in a solution of 4% paraformaldehyde in 0.1 M phosphate buffered saline (pH 7.4) overnight at 4°C. After fixation, slices were incubated in a solution containing 2% Triton X-100 (TX-100), 2% BSA and 5% normal donkey serum

(NDS) in Tris-buffered saline (TBS) at pH 7.4 for 2 h at room temperature to permeabilize and to block nonspecific binding of the primary antibodies. Biocytin-filled networks were visualized with Cy3-conjugated streptavidin (1:200; Jackson ImmunoResearch, Hamburg, Germany). In addition, rabbit anti-BT-IgSF (Rb95) and guinea pig anti-GFAP antibodies were applied to label BT-IgSF and astrocytes, respectively. The floating slices were incubated with primary antibodies for 48 h at 4°C followed by secondary antibodies and DAPI. For additional antibodies see Table S1.

Slices were rinsed and mounted with Aqua Poly/Mount (Polysciences Inc., Washington, USA). Images were acquired by a Leica DM TCS SPE confocal microscope (Leica, Solms, Germany) with Leica software (LCS Lite or LAS AF Lite, respectively). Images were analyzed by ImageJ (FIJI) software, using the cell counter plugin and z-axis projection functions.

Statistics

Results are given as mean ± standard error of the mean (SEM). Data were tested using Mann-Whitney U-test using GraphPad Prism software after excluding outlier by outlier test (ROUT, Q=1%).

Acknowledgements:

We thank Mechthild Henning for technical assistance and Karola Bach, Stefanie Rode and Petra Stallerow for mouse breeding. We thank Dr. Thomas Müller (MDC) with the help in assembling Figure 4. We thank Dr Christopher Patzke (University of Notre Dame, USA) for the critical reading of the manuscript. FGR is an emeritus professor at the MDC. This work was supported in part by funds from the Deutsche Forschungsgemeinschaft SFB 665 to FGR and KE329/28 to HK.

Author contributions

LP, LD, NK, GS, NM, EL, IL, RJ and FGR performed experiments, RJ, HK, CB and FGR evaluated data. FGR drafted and wrote the final version of the manuscript.

Conflict of interest statement: “The authors declare no competing financial interests”

Figures

Figure 1

Expression of BT-IgSF on astrocytes.

A) Localization of BT-IgSF in hippocampus cells from P2-old mice cultured for 10 days in vitro and stained by guinea pig antibodies to GFAP and rabbit anti-BT-IgSF. Scale bar, 20 µm.
B) Western blot of extracts from an astrocyte culture using rabbit antibodies to BT-IgSF. Molecular mass markers are indicated at the left of the panel.
C) Cultured hippocampus cells were stained by antibodies to MAP2a/b and rabbit anti-BT-IgSF. Scale bar, 30 µm. BT-IgSF is found on GFAP astrocytes but rarely detectable on MAP2a/b-positive neurons by antibodies.
D) Localization of BT-IgSF in a coronal hippocampus section from an adult mouse. BT-IgSF is primarily found in the molecular layer and the subgranular zone. Higher magnification shows a widespread localization in the molecular layer probably not restricted to a specific cell type. CA1, cornus ammonis 1; CA3, Cornus ammonis 3; DG, dendate gyrus; GCL, granule cell layer; ML, molecular layer. Left and middle panel, scale bar 1 mm; right panel 20 µm.
E) RNAscope of a coronal section of the hippocampus at P 20 showing expression of BT-IgSF in GFAP-positive astrocytes in the molecular layer and hilus of the dentate gyrus. Scale bar, 50 µm.
F) Higher magnifications of squares as indicated in E). Scale bar, 5 µm.
G) Effective extraction of BT-IgSF from tissues requires SDS. Equal amounts of crude membrane fractions from brain (P56) were extracted with 1% TX100 or SDS. For specificity of the antibody knockout brain tissue is shown.
H) Different postnatal stages of brain extracts obtained by using SDS stained with anti-BT-IgSF are shown. BT-IgSF is primarily found at advanced postnatal stages. Anti-GAPDH indicates equal loading.

Figure 2

Impaired clustering of connexin43 in astrocytes in the absence of BT-IgSF.

A and B) Overview of the location of connexin43 in coronal sections of the hippocampus from wild type (A) and BT-IgSF-deficient (B) mice. 10 weeks old animals were used. CA1, cornus ammonis 1; CA3, Cornus ammonis 3; DG, dendate gyrus; GCL, granule cell layer; ML, molecular layer. Scale bar, 100 µm.
C) Higher magnification of the molecular layer of the dentate gyrus from adult wild type and knockout mice stained by mAb anti-connexin43, rabbit anti-BT-IgSF and DAPI. Arrow heads indicate large connexin43 clusters.
D) Cortical astrocyte monolayer cultures from P3 wildtype or knockout mice at DIV14 stained by mAb anti-connexin43, rabbit anti-BT-IgSF and DAPI. Scale bar, 20µm.

E and F) Quantification of the connexin43 spots and cluster size on astrocytes in the hippocampus.
H and I) Quantification of the connexin43 spots and cluster size of connexin43 on cultured astrocytes.
G and J) Cluster size distribution of connexin43 versus cluster number in the hippocampus or on astrocytes in culture.

Figure 3

Connexin43 but not connexin30 proteins are reduced in the hippocampus and cortex in the absence of BT-IgSF

A and B) Western blots demonstrating reduction of connexin43 in crude membrane fractions from 8 weeks-old hippocampi or cortices of wild type and BT-IgSF-deficient mice. The crude membrane fractions were first solubilized in 1% Triton X100 and unsolubilized material was then solved in 1% SDS. 20 µg of protein was loaded per lane. Loading control is demonstrated by a monoclonal antibody to the heavy chain of clathrin. Quantification of band intensities are shown in B). Blot intensities of the BT-IgSF mutant were normalized to control values. For comparison Western blots of antibodies to connexin30 are shown.
C) The localization of connexin30 in the molecular layer of hippocampi is not affected by the absence of BT-IgSF. DG, dentate gyrus; ML, molecular layer. Scale bar, 20 µm.
D) The expression of GFAP is not reduced in the absence of BT-IgSF. Equal loading is indicated by an antibody to GAPDH.

Figure 4

Impaired gap junction mediated coupling between astrocyte networks in the BT-IgSF knockout mice

A) Scheme of the dye filling experiment to study gap junctional communication in astrocytes.
B) z-stack images of both genotypes of the immunohistochemical analysis for DAPI, biocytin, BT-IgSF and GFAP staining in hippocampus. The right images show an overlay of all channels. GCL, granular cell layer; ML, molecular layer. Bar, 100 µm.
C - E) Scatter plots showing the network size (C, number of coupled cells), tracer spread alongside (D, tracer-spread x) or perpendicular to the Schaffer collaterals (E, tracer-spread y) of each dye-filled hippocampus slice.
F – H) Scatter blots of dye-coupling of astrocytes in the cortex.
I) The density of astrocytes is not reduced in the absence of BT-IgSF. GFAP-positive cells were counted in microscopic view fields (350 µm x 350 µm) in the molecular layer of sections of hippocampi from wild type and BT-IgSF knockout mice. 964 cells in 15 view fields and 616 cells in 9 view fields were counted for wild type and knockout, respectively.
J) Images of GFAP-positive astrocytes in the molecular layer of the hippocampus from wild type and BT-IgSF-deficient mice indicating a similar morphology.

K) Branching of GFAP-positive cells remains unchanged in the absence of BT-IgSF. Primary GFAP-positive branches were counted in the molecular layer of the hippocampus. 46 and 41 cells were counted for wildtype and knockout, respectively.

Figure 5

Expression of BT-IgSF on ependymal cells and impaired localization of connexin43 on ependymal cells in the absence of BT-IgSF

A) Expression of BT-IgSF in ependymal cells of the lateral, third ventricle and central canal by immunohistochemistry using an antibody to the extracellular domain of BT-IgSF. E15 lateral ventricle, scale bar 400 µm; P7 third ventricle, 50 µm; central canal of an E12.5 spinal cord, transversal section; dorsal is up, scale bar 100 µm. Red, anti-BT-IgSF; blue, DAPI. For specificity of the antibody sections of BT-IgSF knockout tissue are shown.
B) Higher magnification of the ependymal cell layer showing expression of BT-IgSF at lateral and basal sides of ependymal cells in the lateral ventricle of an adult wild type mouse. Co-localization of BT-IgSF and GFAP in the ependyma is shown. Ventricle is at the bottom of the image. Scale bar, 20 µm.
C) BT-IgSF is not or only weakly found at the choroid plexus in contrast to the related CAR. Coronal sections from regions of the lateral ventricle from a 19-week-old mouse were stained with rabbit antibodies to BT-IgSF (Rb95) or to CAR (Rb80) and DAPI.
D) Clustering of connexin43 on ependymal cells of the lateral ventricle from adult wild type and BT-IgSF knockout mice. Ventricle is at the top of the images. Arrow heads indicate large connexin43 cluster. Scale bar, 20 µm.
E - G) Quantification of the number of connexin43 spots, size and distribution of number versus size as described for astrocytes.

Figure 6

Connexin36 localization on neurons is not impaired in the absence of BT-IgSF

A - D) Specificity of antibodies to connexin36 in Western blots using crude membrane fractions from wildtype and connexin36-deficient P10 hindbrains. 12 µg of protein was loaded per lane. In A) mAb to connexin36 (sc-398063), in B) mAb to connexin36 (8F6.2), in C) rabbit to connexin36 (364600) and in D) rabbit antibody to connexin36 (amino acid residues 99 to 197) are shown (arrow). Satisfactory specificity could only be demonstrated for antibody shown in D). A 34 kD protein was specifically detected in wild type but not in connexin36-deficient tissue. However, a prominent unspecific band at 52 kD was detected in both genotypes.
E) Specificity of rabbit antibody to connexin36 (residues 99 to 197) in sagittal sections of P10 superior colliculus from wild type and connexin36-deficient mice. Nf, neurofilament.
F) RNAscope demonstrating neuronal expression of BT-IgSF in sagittal sections from P10 superior colliculus.
G) Localization of clustering of connexin36 is not altered in P10 sagittal sections in the absence of BT-IgSF. Scale bar, 20µm. Nf, neurofilament

H) Connexin36 protein is not altered at the protein level in the absence of BT-IgSF.

Supplementary information

Figure S1

Localization of BT-IgSF in the hippocampus at P14 and P80 and demonstration of the specificity of rabbit anti-BT-IgSF.

Coronal cryostat sections of the hippocampus at P14 (A) or P80 (B) were stained with anti-BT-IgSF (Rb95; 1 µg/ml). The dashed boxes indicate the position of the enlarged region shown below row 1 and 3. Absence of staining in BT-IgSF knockout tissues indicates the specificity of rabbit antibodies to BT-IgSF.
CA1, cornus ammonis 1; CA3, Cornus ammonis 3; DG, dentate gyrus; GCL, granule cell layer; ML, molecular layer. Scale bar first and third row, 1 mm; scale bar second and fourth row, 20 µm.

Figure S2

Analysis of dye spreading in astrocytes

A) Bright field and fluorescence images of a patch-clamped astrocyte in the hippocampus. *Top* Sulforhodamine (SR101) staining of the patched astrocyte. The patch-clamp pipettes outline is marked as a dotted line. *Middle* Bright field (BF) image of the field of interest. The arrow marks the position of the patched astrocyte. *Bottom* To ensure success of the dialysis, Lucifer yellow (LY) was added to the pipette-solution. Bar, 20µm.
B) The insets show the typical current profiles of an astrocyte in the wild type (top) or knockout group (bottom) clamped at -70 mV in response to 10 de- and hyperpolarizing voltage-steps in hippocampus. Only cells which displayed a series resistance of ≤ 125% of the initial value after 20 min of dialysis were included in the analysis.
C) The graph shows the averaged current to voltage relationship of both genotypes at the start and the end of the 20 min dialysis period in hippocampus (black: wild type, grey: BT-IgSF knockout).
D) The boxplot graphs compare the membrane capacitance and membrane resistance of hippocampal astrocytes at the start and the end of the dialysis. No significant differences were observed in either comparison (2-way ANOVA, $p > 0.05$). Similar results on the current profiles, membrane capacitance and membrane resistance were obtained from cortical astrocytes (not shown).

Figure S3

Localization of BT-IgSF at the lateral ventricle at P14 and P80.

A and B) Coronal sections of the brain at P14 and P80 were stained with rabbit anti-BT-IgSF. BT-IgSF is strongly localized in cells lining the lateral ventricle. The dashed boxes indicate the position shown in row two or three. Absence of staining in BT-IgSF knockout tissues

indicates the specificity of antibodies to BT-IgSF. LV, lateral ventricle. Scale bar, first and third row, 1 mm; scale bar second and fourth row, 20 µm.

Figure S4

BT-IgSF encoding mRNA is expressed in excitatory and inhibitory neurons of the hippocampus

A) Overview of an RNA scope of BT-IgSF of a coronal section of a P20 hippocampus showing BT-IgSF mRNA encoding cells in all cell layers. Scale bar 500 µm.
B) RNAscope of coronal sections of hippocampi at postnatal day 20 showing expression of BT-IgSF in GFAP-positive astrocytes.
C) RNAscope of coronal sections of hippocampi at postnatal day 20 showing expression of BT-IgSF in vGlut1-positive neurons.
D) RNAscope of coronal sections of hippocampi at postnatal day 20 showing expression of BT-IgSF in GAD65-positive neurons.

Table S1: Antibodies for immunohistochemistry, immunocytochemistry and for Western blotting

Antibody	IHC and ICC	Western blots	Source
Rabbit anti-BT-IgSF-Fc (Rb95 or Rb96) IgG	1-3 µg/ml	1 µg/ml	Pelz et al., 2017
Rabbit anti-CAR	1 µg/ml		Patzke et al., 2010
mAb anti-connexin43	1 µg/ml		Transduction Laboratories, #610061
Rabbit anti-connexin43	1:200	1:1000	Cell signaling, #3512
Rabbit anti-connexin30	1 µg/ml	0.5 µg/ml	Invitrogen #71-2200
Rabbit anti-connexin36		1 µg/ml	Zymed/Invitrogen 36-4600
mAb connexin36 (H9)		1 µg/ml	Santa Cruz sc-398063
Rabbit anti-connexin36 (RbB5)	0.5 µg/ml	0.5 µg/ml	This study
mAb α-Tubulin		0.025 µg/ml	Calbiochem CP06
mAb anti-neurofilament	7.5 µg/ml		mAb 2H3 Developmental Hybridoma Bank
mAb connexin35/36		1 µg/ml	Millipore MAB3045

Guinea pig anti-GFAP	1:500	1:1000	Synaptic Systems#173004
Goat anti-GFAP	1:200	1:1000	Santa Cruz #sc-6170
Rabbit anti-GFAP	1:1000		Dako Z0334
mAb anti-MAP2a/b	1:500	1:1000	Dianova#DLN-08583
mAb anti-ZO-1	5 µg/ml		Invitrogen #339100
Rabbit anti-ZO-1	1:100		Invitrogen #40-2200
mAb anti-GAPDH (1D4)		0.5 µg/ml	Novus Biologicals, #NB300-221
mAb anti-Clathrin (heavy chain)		1:1000	BD Transduction Laboratories #610499
Goat anti-Rabbit-Cy3	1:400 – 1:1000		Dianova
Goat anti-Mouse-Alexa488	1:400 – 1:1000		Molecular Probes
Rabbit anti-Goat-Alexa488	1:500		
Goat anti-Rabbit-HRP		1:20 000	Dianova
Goat anti-Mouse-HRP		1:20 000	Dianova

References

Ahi, E. P. and Sefc, K. M. (2017). A gene expression study of dorso-ventrally restricted pigment pattern in adult fins of Neolamprologus meeli, an African cichlid species. *PeerJ* **5**, e2843.

Baldwin, K. T., Tan, C. X., Strader, S. T., Jiang, C., Savage, J. T., Elorza-Vidal, X., Contreras, X., Rülicke, T., Hippenmeyer, S., Estévez, R., et al. (2021). HepaCAM controls astrocyte self-organization and coupling. *Neuron* **109**, 2427-2442.e10.

Bock, M. De, Kerrebrouck, M., Wang, N. and Leybaert, L. (2013). Neurological manifestations of oculodentodigital dysplasia: A Cx43 channelopathy of the central nervous system? *Front. Pharmacol.* **4 SEP**, 1–21.

Charvériat, M., Naus, C. C., Leybaert, L. and Sáez, J. C. (2017). Connexin-Dependent Neuroglial Networking as a New Therapeutic Target. **11**,.

Chen, B., Zhu, G., Yan, A., He, J., Liu, Y., Li, L., Yang, X., Dong, C. and Kee, K. (2021). IGSF11 is required for pericentric heterochromatin dissociation during meiotic diplotene. *PLoS Genet.* **17**,.

Condorelli, D. F., Parenti, R., Spinella, F., Salinaro, A. T., Belluardo, N., Cardile, V. and Cicirata, F. (1998). Cloning of a new gap junction gene (Cx36) highly expressed in mammalian brain neurons. *Eur. J. Neurosci.* **10**, 1202–1208.

Degen, J., Meier, C., Van Der Giessen, R. S., Söhl, G., Petrasch-Parwez, E., Urschel, S., Dermietzel, R., Schilling, K., De Zeeuw, C. I. and Willecke, K. (2004). Expression Pattern of lacZ Reporter Gene Representing Connexin36 in Transgenic Mice. *J. Comp. Neurol.* **473**, 511–525.

Dermietzel, R., Traub, O., Hwang, T. K., Beyer, E., Bennett, M. V, Spray, D. C. and Willecke, K. (1989). Differential expression of three gap junction proteins in developing and mature brain tissues. *Proc. Natl. Acad. Sci. U. S. A.* **86**, 10148–10152.

Deshpande, T., Li, T., Henning, L., Wu, Z., Müller, J., Seifert, G., Steinhäuser, C. and Bedner, P. (2020). Constitutive deletion of astrocytic connexins aggravates kainate-induced epilepsy. *Glia* **68**, 2136–2147.

Duffy, H. S., Delmar, M. and Spray, D. C. (2002). Formation of the gap junction nexus: binding partners for connexins. *J. Physiol.* **96**, 243–249.

Eom, D. S., Inoue, S., Patterson, L. B., Gordon, T. N., Slingwine, R., Kondo, S., Watanabe, M. and Parichy, D. M. (2012). Melanophore Migration and Survival during Zebrafish Adult Pigment Stripe Development Require the Immunoglobulin Superfamily Adhesion Molecule Igsf11. *PLoS.Genet.* **8**, e1002899.

Falk, M. M. (2020). Do CAR and CAR family members aid in gap junction formation? *BioEssays* 2000276.

Fischer, G. and Kettenmann, H. (1985). Cultured astrocytes form a syncytium after maturation. *Exp. Cell Res.* **159**, 273–279.

Giaume, C., Koulakoff, A., Roux, L., Holcman, D. and Rouach, N. (2010). Astroglial networks: A step further in neuroglial and gliovascular interactions. *Nat. Rev. Neurosci.* **11**, 87–99.

Güldenagel, M., Ammermüller, J., Feigenspan, A., Teubner, B., Degen, J., Söhl, G., Willecke, K. and Weiler, R. (2001). Visual transmission deficits in mice with targeted disruption of the gap junction gene connexin36. *J. Neurosci.* **21**, 6036–6044.

Gulisano, M., Parenti, R., Spinella, F. and Cicirata, F. (2000). Cx36 is dynamically expressed during early development of mouse brain and nervous system. *Neuroreport* **11**, 3823–3828.

Haffter, P., Odenthal, J., Mullins, M. C., Lin, S., Farrell, M. J., Vogelsang, E., Haas, F., Brand, M., van Eeden, F. J., Furutani-Seiki, M., et al. (1996). Mutations affecting pigmentation and shape of the adult zebrafish. *Dev. Genes Evol.* **206**, 260–276.

Harada, H., Suzu, S., Hayashi, Y. and Okada, S. (2005). BT-IgSF, a novel immunoglobulin superfamily protein, functions as a cell adhesion molecule. *J.Cell Physiol* **204**, 919–926.

Hardy, E., Rancillac, A., Cohen-salmon, M. and Rouach, N. (2021). Astroglial Cx30 differentially impacts synaptic activity from hippocampal principal cells and interneurons. 1–21.

Hayano, Y., Ishino, Y., Hyun, J. H., Orozco, C. G., Steinecke, A., Potts, E., Oisi, Y., Thomas, C. I., Guerrero-Given, D., Kim, E., et al. (2021). IgSF11 homophilic adhesion proteins promote layer-specific synaptic assembly of the cortical interneuron subtype. *Sci. Adv.* **7**,.

Hervé, J. C., Derangeon, M., Sarrouilhe, D. and Bourmeyster, N. (2014). Influence of the scaffolding protein Zonula Occludens (ZOs) on membrane channels. *Biochim. Biophys. Acta - Biomembr.* **1838**, 595–604.

Higashine, K., Hashimoto, K., Tsujimoto, E., Oishi, Y., Hayashi, Y. and Miyamoto, Y. (2018). Promotion of differentiation in developing mouse cerebellar granule cells by a cell adhesion molecule BT-IgSF. *Neurosci. Lett.* **686**, 87–93.

Huang, X., Su, Y., Wang, N., Li, H., Li, Z., Yin, G., Chen, H., Niu, J. and Yi, C. (2021). Astroglial Connexins in Neurodegenerative Diseases. *Front. Mol. Neurosci.* **14**, 1–9.

Hunter, A. W., Barker, R. J., Zhu, C. and Gourdie, R. G. (2005). Zonula occludens-1 alters connexin43 gap junction size and organization by influencing channel accretion. *Mol. Biol. Cell* **16**, 5686–5698.

Irion, U., Frohnhofer, H. G., Krauss, J., Colak Champollion, T., Maischein, H.-M., Geiger-Rudolph, S., Weiler, C. and Nusslein-Volhard, C. (2014). Gap junctions composed of connexins 41.8 and 39.4 are essential for colour pattern formation in zebrafish. *Elife* **3**, e05125.

Jang, S., Oh, D., Lee, Y., Hosy, E., Shin, H., van Riesen, C., Whitcomb, D., Warburton, J. M., Jo, J., Kim, D., et al. (2015). Synaptic adhesion molecule IgSF11 regulates synaptic transmission and plasticity. *Nat. Neurosci.* **19**, 84–93.

Katoh, M. M. and Katoh, M. M. (2003). IGSF11 gene, frequently up-regulated in intestinal-type gastric cancer, encodes adhesion molecule homologous to CXADR, FLJ22415 and ESAM. *Int J Oncol* **23**, 525–531.

Kettenmann, H., Orkand, R. K. and Schachner, M. (1983). Coupling among identified cells in mammalian nervous system cultures. *J. Neurosci. Off. J. Soc. Neurosci.* **3**, 506–516.

Kim, H., Takegahara, N., Walsh, M. C., Middleton, S. A., Yu, J., Shirakawa, J., Ueda, J., Fujihara, Y., Ikawa, M., Ishii, M., et al. (2020). IgSF11 regulates osteoclast differentiation through association with the scaffold protein PSD-95. *Bone Res.* **8**, 5.

Laing, J. G., Chou, B. C. and Steinberg, T. H. (2005). ZO-1 alters the plasma membrane localization and function of Cx43 in osteoblastic cells. *J. Cell Sci.* **118**, 2167–2176.

Langhorst, H., Jüttner, R., Groneberg, D., Mohtashamdolatshahi, A., Pelz, L., Purfürst, B., Schmidt-Ott, K. M., Friebe, A., Rathjen, F. G., Juttner, R., et al. (2018). The IgCAM CLMP regulates expression of Connexin43 and Connexin45 in intestinal and ureteral smooth muscle contraction in mice. *Dis. Model. Mech.* **11**, dmm032128.

Li, M. W. M., Mruk, D. D., Lee, W. M. and Cheng, C. Y. (2010). Connexin 43 is critical to maintain the homeostasis of the blood-testis barrier via its effects on tight junction reassembly. *Proc. Natl. Acad. Sci. U. S. A.* **107**, 17998–18003.

Lim, B. K., Xiong, D., Dorner, A., Youn, T. J., Yung, A., Liu, T. I., Gu, Y., Dalton, N. D., Wright, A. T., Evans, S. M., et al. (2008). Coxsackievirus and adenovirus receptor (CAR) mediates atrioventricular-node function and connexin 45 localization in the murine heart. *J.Clin.Invest* **118**, 2758–2770.

Lisewski, U., Shi, Y., Wrackmeyer, U., Fischer, R., Chen, C., Schirdewan, A., Juttner,

R., Rathjen, F., Poller, W., Radke, M. H., et al. (2008). The tight junction protein CAR regulates cardiac conduction and cell-cell communication. *J.Exp.Med.* **205**, 2369–2379.

Lutz, S. E., Zhao, Y., Gulinello, M., Lee, S. C., Raine, C. S. and Brosnan, C. F. (2009). Deletion of astrocyte connexins 43 and 30 leads to a dysmyelinating phenotype and hippocampal CA1 vacuolation. *J. Neurosci.* **29**, 7743–7752.

Maglione, M., Tress, O., Haas, B., Karram, K., Trotter, J., Willecke, K., Kettenmann, H., Trotter, J., Maglione, M., Karram, K., et al. (2010). Oligodendrocytes in mouse corpus callosum are coupled via gap junction channels formed by connexin47 and connexin32. *Glia* **58**, 1104–1117.

Mayorquin, L. C., Rodriguez, A. V., Sutachan, J. J. and Albarracín, S. L. (2018). Connexin-mediated functional and metabolic coupling between astrocytes and neurons. *Front. Mol. Neurosci.* **11**, 1–10.

Mazaud, D., Capano, A. and Rouach, N. (2021). The many ways astroglial connexins regulate neurotransmission and behavior. *Glia* **69**, 2527–2545.

McCarthy, K. and De Vellis, J. (1980). Preparation of separate astroglial and oligodendroglial cell cultures from rat cerebral tissue. *J.Cell Biol.* **85**, 890–902.

Molofsk, A. V., Krenick, R., Ullian, E., Tsai, H. H., Deneen, B., Richardson, W. D., Barres, B. A. and Rowitch, D. H. (2012). Astrocytes and disease: A neurodevelopmental perspective. *Genes Dev.* **26**, 891–907.

Nagy, J. I., Dudek, F. E. and Rash, J. E. (2004). Update on connexins and gap junctions in neurons and glia in the mammalian nervous system. *Brain Res. Rev.* **47**, 191–215.

Pannasch, U., Vargova, L., Reingruber, J., Ezan, P., Holcman, D., Giaume, C., Sykova, E. and Rouach, N. (2011). Astroglial networks scale synaptic activity and plasticity. *Proc. Natl. Acad. Sci.* **108**, 8467–8472.

Pelz, L., Purfürst, B. and Rathjen, F. G. (2017). The cell adhesion molecule BT-IgSF is essential for a functional blood-testis barrier and male fertility in mice. *J. Biol. Chem.* **292**, 21490–21503.

Perea, G., Navarrete, M. and Araque, A. (2009). Tripartite synapses: astrocytes process and control synaptic information. *Trends Neurosci.* **32**, 421–431.

Pereda, A. E. (2014). Electrical synapses and their functional interactions with chemical synapses. *Nat. Rev. Neurosci.* **15**, 250–263.

Rathjen, F. G. (2020). The CAR group of Ig cell adhesion proteins – Regulators of gap junctions ? 1–11.

Rhett, J. M., Jourdan, J. and Gourdie, R. G. (2008). Connexin 43 connexon to gap junction transition is regulated by zonula occludens-1.

Richter, N., Wendt, S., Georgieva, P. B., Hambardzumyan, D., Nolte, C. and Kettenmann, H. (2014). Glioma-associated microglia and macrophages/monocytes display distinct electrophysiological properties and do not communicate via gap junctions. *Neurosci. Lett.* **583**, 130–135.

Rubio, M. E. and Nagy, J. I. (2015). Connexin36 expression in major centers of the auditory system in the CNS of mouse and rat: Evidence for neurons forming purely electrical synapses and morphologically mixed synapses. *Neuroscience* **303**, 604–629.

Saunders, N. R., Dziegielewska, K. M., Møllgård, K. and Habgood, M. D. (2018). Physiology and molecular biology of barrier mechanisms in the fetal and neonatal brain. *J. Physiol.* **596**, 5723–5756.

Singh, A. P. and Nusslein-Volhard, C. (2015). Zebrafish stripes as a model for vertebrate colour pattern formation. *Curr. Biol.* **25**, R81–R92.

Söhl, G., Degen, J., Teubner, B. and Willecke, K. (1998). The murine gap junction gene connexin36 is highly expressed in mouse retina and regulated during brain development. *FEBS Lett.* **428**, 27–31.

Solan, J. L. and Lampe, P. D. (2016). Kinase programs spatiotemporally regulate gap junction assembly and disassembly: Effects on wound repair. *Semin. Dev.Biol.* **50**, 40–48.

Spassky, N. and Meunier, A. (2017). The development and functions of multiciliated epithelia. *Nat. Rev. Mol. Cell Biol.* **18**, 423–436.

Steinhäuser, C. and Boison, D. (2012). Epilepsy: Crucial role for astrocytes. *Glia* **60**, 1191.

Suzu, S., Hayashi, Y., Harumi, T., Nomaguchi, K., Yamada, M., Hayasawa, H. and Motoyoshi, K. (2002). Molecular cloning of a novel immunoglobulin superfamily gene preferentially expressed by brain and testis. *Biochem.Biophys.Res.Commun.* **296**, 1215–1221.

Tan, C. X., Burrus Lane, C. J. and Eroglu, C. (2021). *Role of astrocytes in synapse formation and maturation*. 1st ed. Elsevier Inc.

Theis, M., Jauch, R., Zhuo, L., Speidel, D., Wallraff, A., Döring, B., Frisch, C., Söhl, G., Teubner, B., Euwens, C., et al. (2003). Accelerated hippocampal spreading depression and enhanced locomotory activity in mice with astrocyte-directed inactivation of connexin43. *J. Neurosci.* **23**, 766–776.

van Steensel, M. A. M., Spruijt, L., van der Burgt, I., Bladergroen, R. S., Vermeer, M., Steijlen, P. M. and van Geel, M. (2005). A 2-bp deletion in the GJA1 gene is associated with oculo-dento-digital dysplasia with palmoplantar keratoderma. *Am. J. Med. Genet. A* **132A**, 171–174.

Ventura, R. and Harris, K. M. (1999). Three-dimensional relationships between hippocampal synapses and astrocytes. *J. Neurosci.* **19**, 6897–6906.

Wang, F., Flanagan, J., Su, N., Wang, L. C., Bui, S., Nielson, A., Wu, X., Vo, H. T., Ma, X. J. and Luo, Y. (2012). RNAscope: A novel in situ RNA analysis platform for formalin-fixed, paraffin-embedded tissues. *J. Mol. Diagnostics* **14**, 22–29.

Wang, J., Wu, G., Manick, B., Hernandez, V., Renelt, M., Erickson, C., Guan, J., Singh, R., Rollins, S., Solorz, A., et al. (2018). VSIG-3 as a ligand of VISTA inhibits human T-cell function. *Immunology*.

Watanabe, M. and Kondo, S. (2012). Changing clothes easily: connexin41.8 regulates skin pattern variation. *Pigment Cell Melanoma Res.* **25**, 326–330.

Watanabe, M., Iwashita, M., Ishii, M., Kurachi, Y., Kawakami, A., Kondo, S. and Okada, N. (2006). Spot pattern of leopard Danio is caused by mutation in the zebrafish connexin41.8 gene. *EMBO Rep.* **7**, 893–897.

Willecke, K., Eiberger, J., Degen, J., Eckardt, D., Romualdi, A., Guldenagel, M., Deutsch, U. and Sohl, G. (2002). Structural and functional diversity of connexin genes in the mouse and human genome. *Biol.Chem.* **383**, 725–737.

Wu, M., Moh, M. C. and Schwarz, H. (2016). HepaCAM associates with connexin 43 and enhances its localization in cellular junctions. *Sci. Rep.* **6**, 36218.

Zhang, J., Chandrasekaran, G., Li, W., Kim, D. Y., Jeong, I. Y., Lee, S. H., Liang, T., Bae, J. Y., Choi, I., Kang, H., et al. (2020). Wnt-PLC-IP3-Connexin-Ca2+ axis maintains ependymal motile cilia in zebrafish spinal cord. *Nat. Commun.* **11**,.

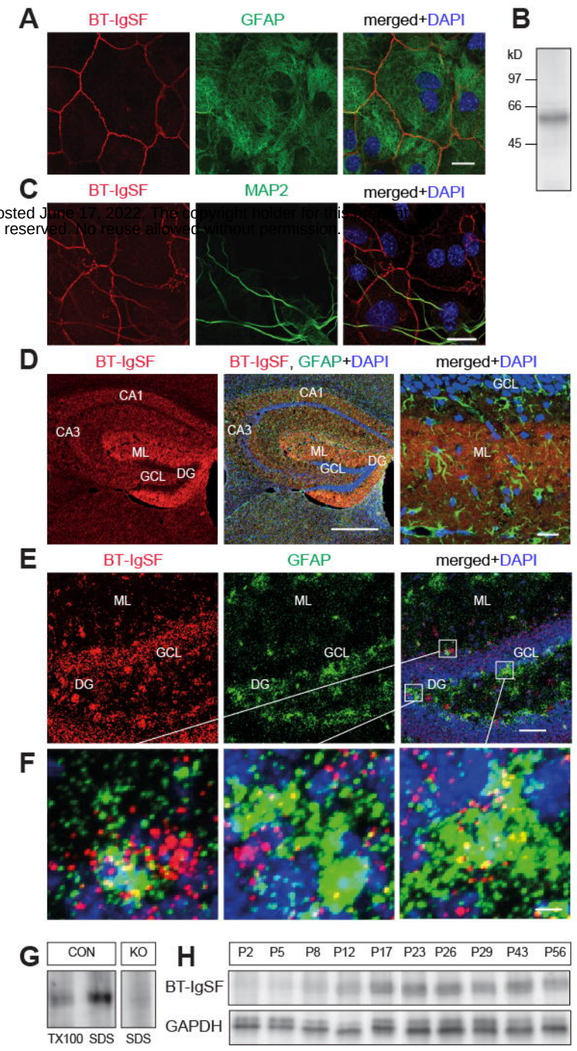

Figure 1: Pelz et al.

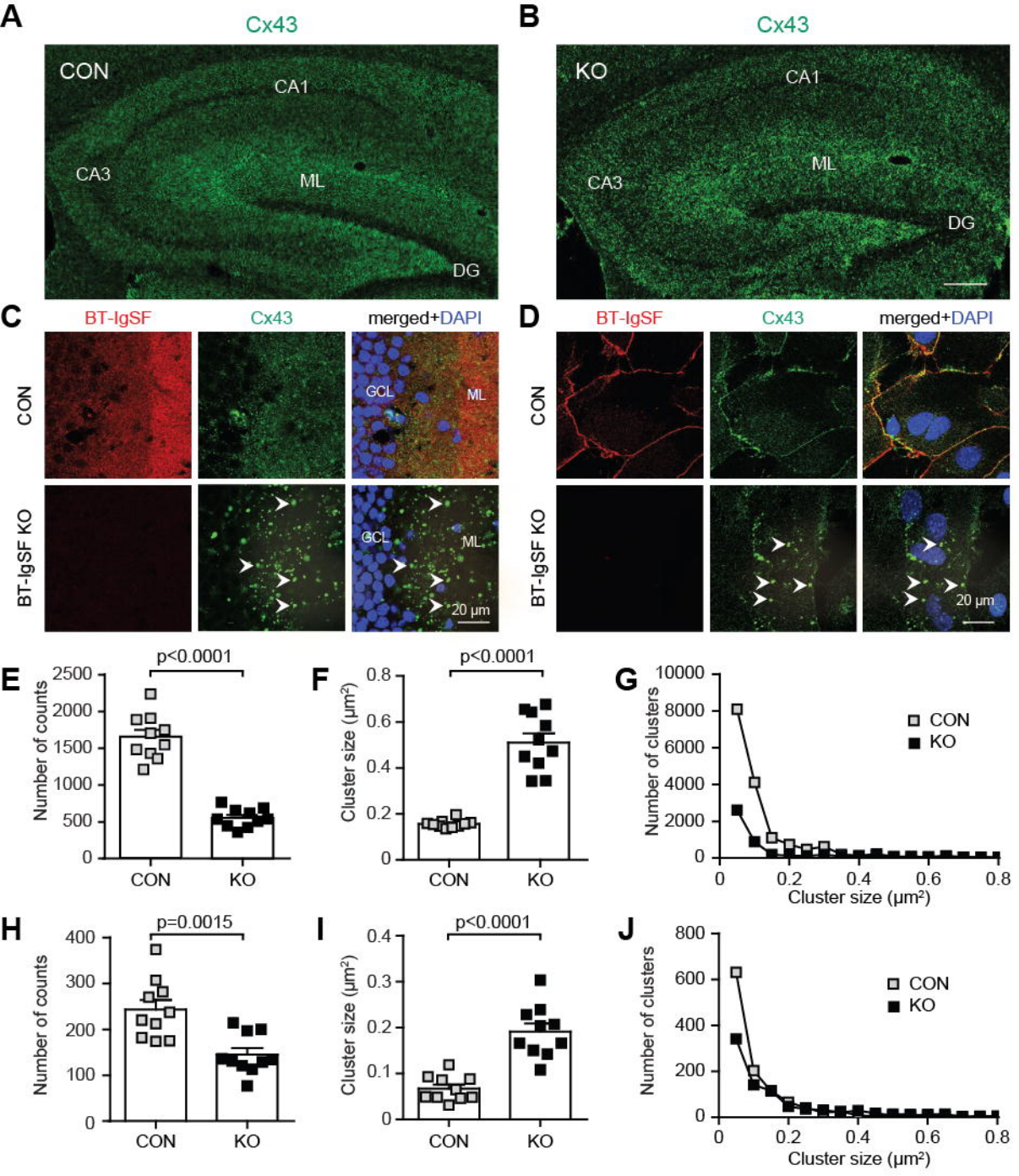

Figure 2: Pelz et al.

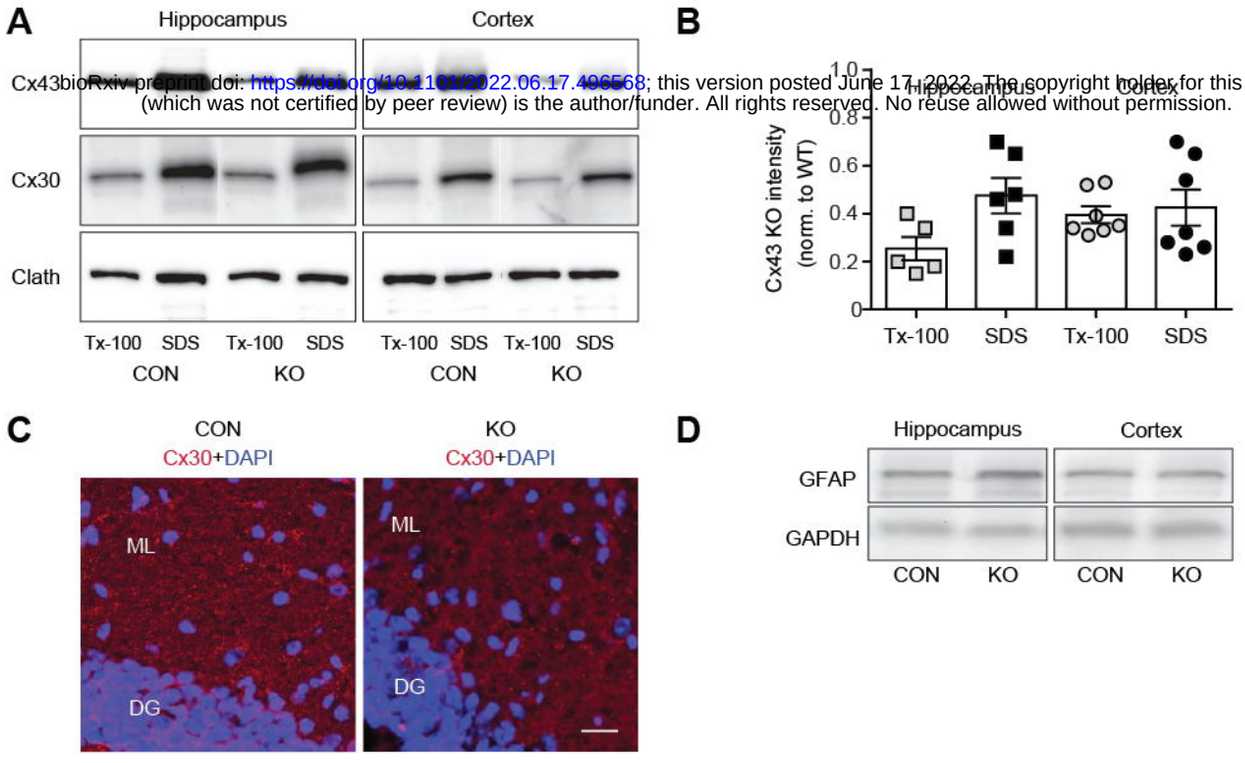

Figure 3: Pelz et al.

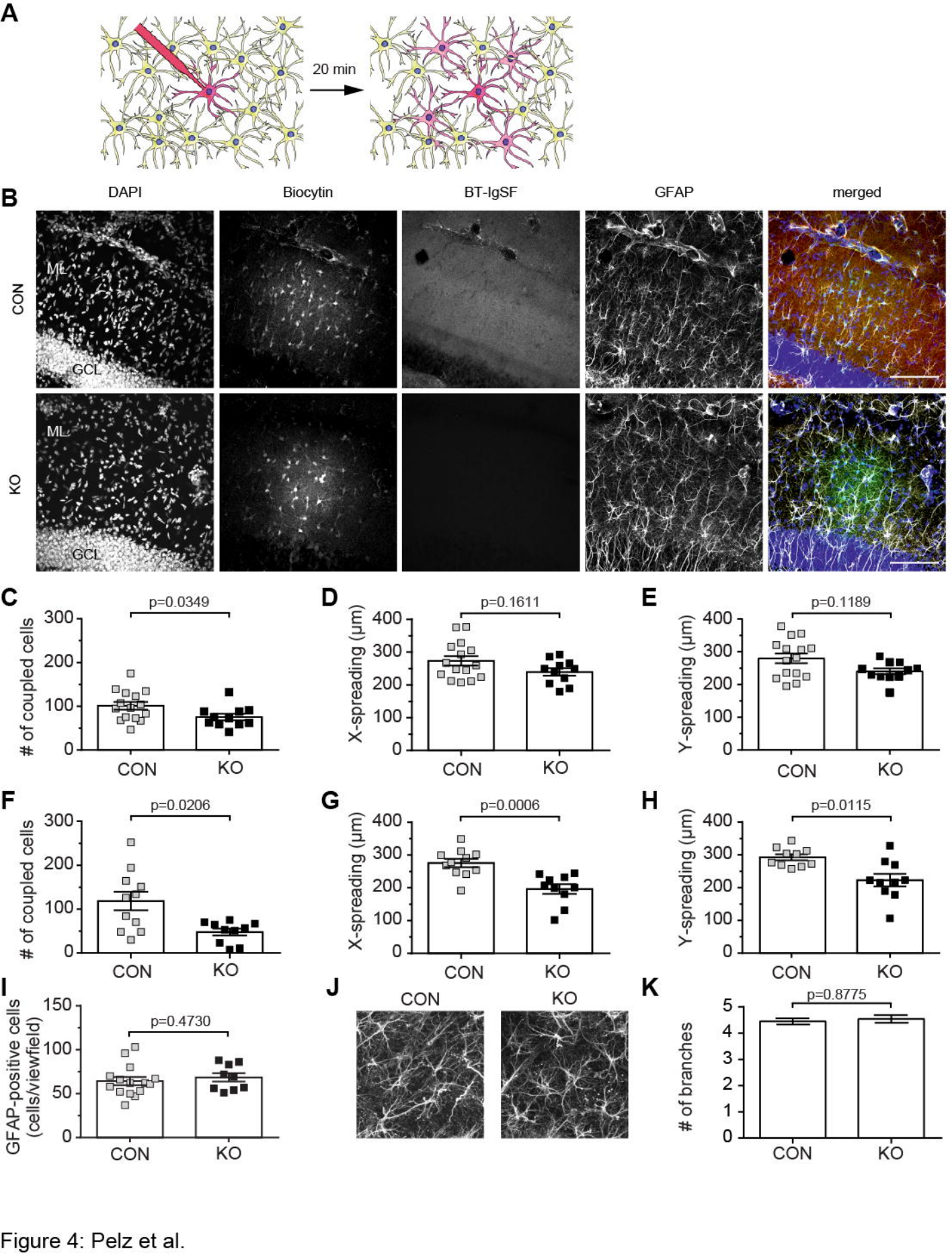

Figure 4: Pelz et al.

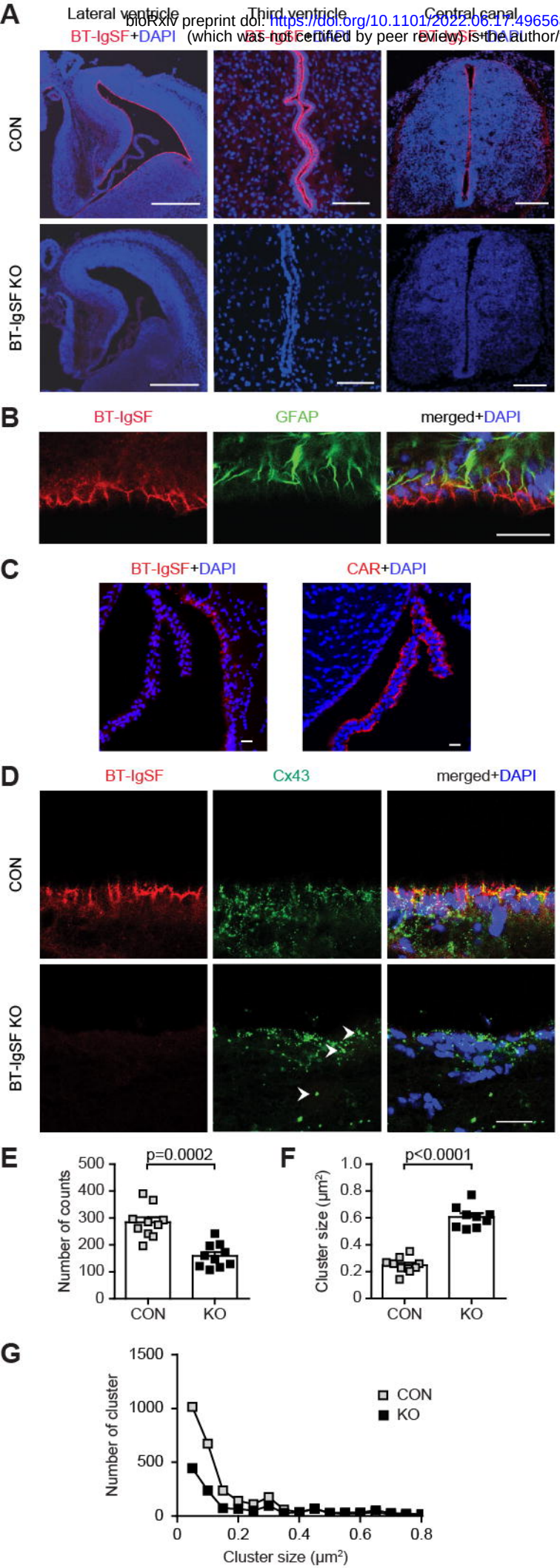

Figure 5: Pelz et al.

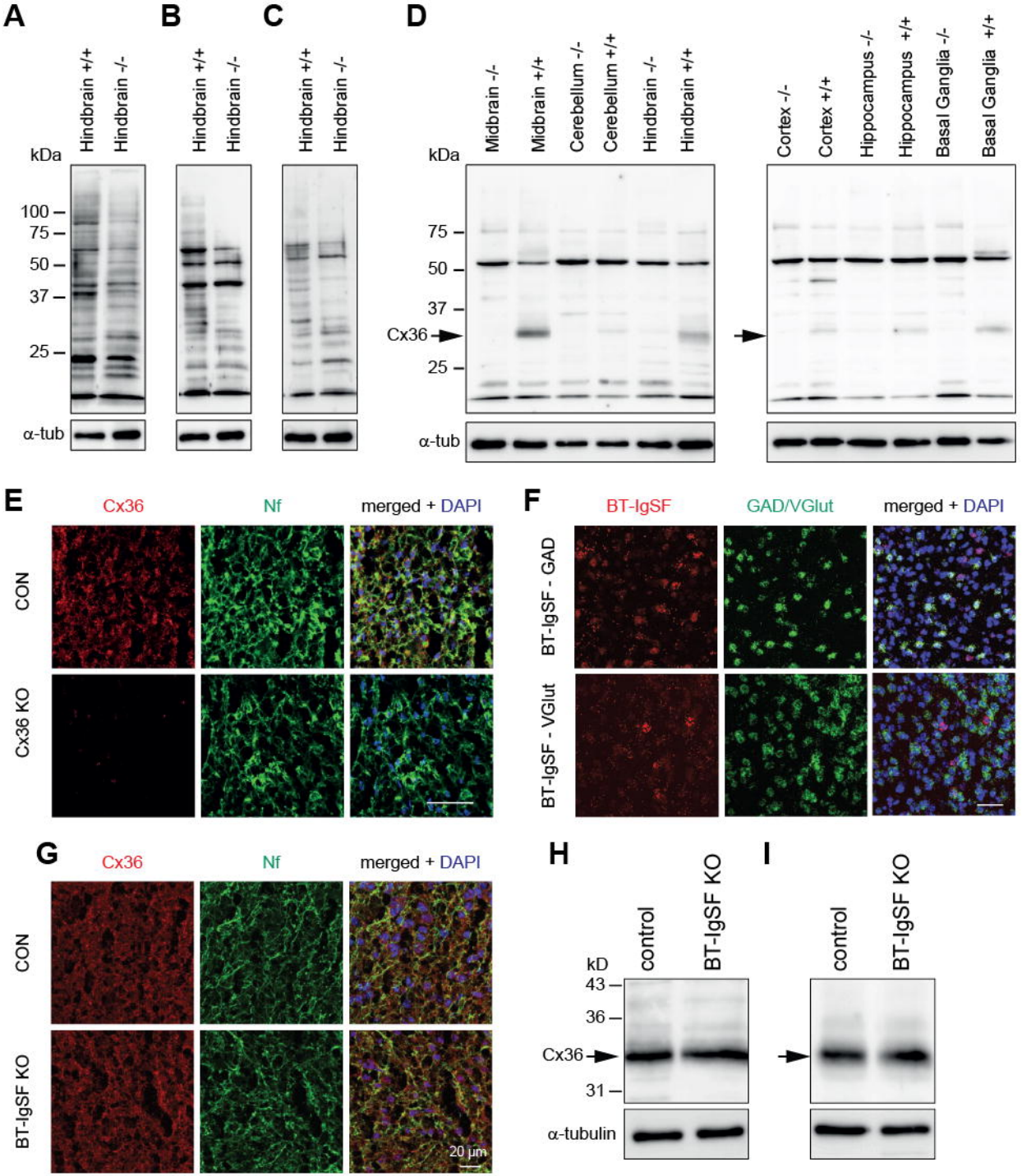

Figure 6: Pelz et al.